Structural covariance networks in the fetal brain reveal altered neurodevelopment for specific subtypes of congenital heart disease

Siân Wilson PhD*[1,2], Daniel Cromb MRCPCH*[1], Alexandra F. Bonthrone PhD[1], Alena Uus PhD[1,3], Anthony Price PhD[1], Alexia Egloff MD[1], Milou P.M Van Poppel MSc[3,4], Johannes K Steinweg MBBS[3,4], Kuberan Pushparajah PhD[3,4], John Simpson FRCP[3,4], David FA Lloyd PhD[3,4], Reza Razavi PhD[3], Jonathan O'Muircheartaigh PhD[1], A. David Edwards DSc[1], Joseph V. Hajnal PhD[1,3], Mary Rutherford FRCR[1], Serena J. Counsell PhD[1]

1. Centre for the Developing Brain, School of Biomedical Engineering and Imaging Sciences, King's College London, UK

2. Fetal and Neonatal Developmental Science Centre, Boston Children's Hospital, Harvard Medical School, Boston, USA.

3. Biomedical Engineering Department, School of Biomedical Engineering and Imaging Sciences, King's College London, London, UK

4. Department of Congenital Heart Disease, Evelina London Children's Hospital, London, UK

*Joint first authorship

Short title:

Structural covariance in fetuses with CHD

Corresponding author:
Professor Serena Counsell
Centre for the Developing Brain, School of Biomedical Engineering & Imaging Sciences
King's College London,
London, SE1 7EH, UK
Email: serena.counsell@kcl.ac.uk

Phone: +44 (0)20 7188 7188 ext. 53612
Fax: +44 (0)20 7188 8154

Word count: 5522

Abstract

Background Altered structural brain development has been identified in fetuses with Congenital Heart Disease (CHD), suggesting that the neurodevelopmental impairment observed later in life might originate in utero. There are many interacting factors that may perturb neurodevelopment during the fetal period and manifest as structural brain alterations, such as altered cerebral substrate delivery and aberrant fetal hemodynamics.

Methods We extracted structural covariance networks (SCNs) from the log Jacobian determinants of 429 in utero T2w MRI scans, (n = 67 controls, 362 CHD) acquired during the third trimester. We fit general linear models to test whether age, sex, expected cerebral substrate delivery and CHD diagnosis were significant predictors of structural covariance.

Results We identified significant effects of age, sex, cerebral substrate delivery, and specific CHD diagnosis across a variety of SCNs, including primary motor and sensory cortices, cerebellar regions, frontal cortex, extra-axial CSF, thalamus, brainstem, and insula, consistent with widespread coordinated aberrant maturation of specific brain regions over the third trimester.

Conclusions SCNs offer a sensitive, data-driven approach to explore whole-brain structural changes without anatomical priors. We used them to stratify a heterogenous CHD patient cohort, highlighting similarities and differences between diagnoses during fetal neurodevelopment. Although there was a clear effect of abnormal fetal hemodynamics on structural brain maturation, our results suggest that this alone does not explain all the variation in brain development between individuals with CHD.

Introduction

Congenital heart disease (CHD) is the most common congenital malformation (EUROCAT 2020), occurring at a frequency of 0.8% to 1.2% of live births worldwide (Dolk et al., 2011, Bouma & Mulder 2017). CHD encompasses a wide spectrum of cardiovascular defects, from simple cardiac malformations to more complex and severe lesions that require surgical intervention. Following improvements in surgical and therapeutic intervention over the last two decades, most patients with CHD will survive into adulthood (Dellborg et al., 2023). However, many will display impairments affecting a wide range of neurodevelopmental domains (Latal et al, 2016, Newburger et al., 2012, Naef et al., 2017, Marelli et al., 2016, Bellinger et al 2011). Research into the mechanisms underpinning impaired neurodevelopment in CHD may enable appropriate preventative prenatal interventions to promote improved neurodevelopmental outcomes later in life.

With recent advances in fetal MRI, it has become possible to study brain development in utero. Previous work has identified deviations from normal brain growth trajectories in fetuses with CHD, including reduced regional brain volumes (Limperopoulos 2010, Clouchoux et al., 2013, Brossard-Racine 2014, Ren et al., 2021, Dovjak et al., 2022, Cromb et al. 2023), altered volumes of transient fetal compartments (Rollins et al., 2021, Wu et al., 2021), reduced cortical folding (Ortinau 2019, Jaimes et al., 2020) and a relationship between cerebral oxygen delivery and fetal brain size (Sun et al., 2015, Cromb et al, 2023). These studies demonstrate that abnormal neurodevelopment in the CHD population begins in utero during a period of rapid brain growth, featuring metabolically demanding cellular processes such as gyrification, oligodendrocyte maturation, and synaptogenesis. It has been hypothesised that aberrant cardiovascular physiology, altering the delivery of oxygen, glucose and other nutrients to the fetal brain during this critical window, impairs brain development (Peyvandi 2021, Lauridsen 2017, Sun 2015). Different types of CHD will affect the pattern of cerebral substrate delivery in different ways, likely having unique implications for brain development (Sun et al., 2021, Rollins

et al., 2021, Cromb et al., 2023). There are also a multitude of other interacting factors that may perturb neurodevelopment during the fetal period and manifest as structural brain alterations. These include genetic factors, placental function, maternal stress, socioeconomic and environmental factors. Disentangling the effect of each of these factors remains a challenge, and therefore our understanding of structural brain abnormalities in the CHD population is incomplete.

In this work, we extracted structural covariance networks (SCNs) from the brain MRI of 429 fetuses. SCNs represent brain regions with coherent structural expansion and coordinated, independent maturational trajectories, often converging on functional brain networks (Geng et al., 2017, Seeley et al., 2009). SCNs have been used effectively to investigate changes in the organization of the brain at the network level, both in healthy ageing populations (Li et al., 2013, Geng et al., 2017, Spreng & Turner 2013), and in at-risk populations including preterm infants (Fenchel et al., 2021, Vanes et al., 2021), psychiatric patient cohorts (Bassett et al., 2008, Heinze et al., 2015), and in neurodegenerative disease (He et al., 2008, Seeley et al., 2009). SCNs offer a data-driven, dimensionality reduction approach, removing the dependency on predefined regions of interest, which allows the examination of dynamic contrast changes across space and time. This is particularly relevant for investigating the maturation of the fetal brain, which is rapid, complex, and characterised by the presence of transient structures (Kostovic & Rakic 1990). This model-free approach is also well suited to studying the heterogenous and varied pathophysiology of CHD, as it extracts features that represent independent modes of variation across the cohort. We hypothesized that by examining the sources of variance, we would be able to disentangle the effect of specific cardiac defects on the developing brain.

To address this challenge, we examined a large cohort of 429 fetuses, including 369 fetuses with CHD. There are many approaches to categorize CHD cohorts (Sun et al., 2015, Roberts et

al., 2020) and explore the interplay between cardiovascular physiology and fetal brain development. For the purpose of this study, we divided the CHD cohort into groups based on the expected effect of the underlying cardiac defect on the streaming of substrate-rich placental blood to the cerebral circulation (Cromb et al., 2023). Each subject was reviewed individually, using fetal phase-contrast MRI flow data and/or contemporaneous echocardiography where available, as published in previous work (Cromb et al., 2023). This categorization was used to the test the specific hypothesis that cerebral substrate delivery affects the co-maturation of SCNs.

We also examined whether gestational age, sex, and CHD diagnosis are underlying sources of variation in structural brain maturation. With this approach, we stratified our large cohort of fetuses with CHD, identifying SCNs that vary across the population according to cerebral substrate delivery and more specifically, CHD diagnosis. We identify networks whose coordinated maturation is different from healthy controls but shared between multiple subtypes of CHD. We also find networks that are uniquely different for specific CHD diagnoses. Overall, this approach identified associations between specific cardiac defects and how they manifest in the developing fetal brain, which offers crucial insight into the potential structural underpinnings of neurodevelopmental abnormalities.

Methods

Ethical approval

The National Research Ethics Service West London committee provided ethical approval (07/H0707/105, 14/LO/1806, 17/LO/0292). Informed written consent was obtained before fetal MRI.

Participants

Mothers were recruited between June 2014 and June 2022 at the Evelina Children's Hospital in London, following routine ultrasound during the second trimester. 529 women (maternal age scan=31.52 (±5.73) years) were carrying a fetus with either known or suspected CHD. Participants were scanned during the third trimester, between 27 and 36 gestational weeks (GW). Exclusion criteria for mothers included multiple pregnancies, maternal weight over 125 kg (at time of scan), maternal diabetes, maternal hypertension, inability to give informed consent, or age under 18 years at the time of referral.

We also excluded fetuses with confirmed genetic diagnosis, such as 22q deletion syndrome, extracardiac anomalies, such as congenital diaphragmatic hernia or duodenal atresia, or structural brain abnormalities reported on fetal MRI, including bilateral ventriculomegaly, cerebellar hypoplasia or absence of the corpus callosum. After applying the exclusion criteria, the cohort consisted of 429 fetal MR scans (including 67 controls, and 362 fetuses diagnosed with CHD).

Image acquisition & reconstruction

All scans were acquired on a Philips Ingenia 1.5T scanner, with 28-channel dStream anterior and posterior built-in coils. The T2-weighted fast-spin-echo sequence was specifically optimised for fetal imaging (TR = 13 ms, TE = 80 ms, image resolution= 1.25x1.25x2.5mm, slice thickness = 2.5 mm, slice spacing = 1.25 mm). A 3D slice-to-volume image reconstruction pipeline (available at https://github.com/SVRTK/SVRTK, https://hub.docker.com/r/fetalsvrtk/svrtk auto2.20) was used for motion correction, reconstructing the T2w images to 0.5mm3 isotropic resolution (Kuklisova-Murgasova 2012, Uus et al., 2021).

MRI Quality control

All MRI scans were reviewed and reported by expert perinatal radiologists. The presence of any structural abnormalities was recorded, and image quality was scored on a scale from 1-4, based on the signal:noise ratio, presence of artefacts, field of view and residual motion (4 = High quality, 3 = Acceptable, 2 = Poor, 1 = Failed). Only subjects scoring 3 or 4 were included in the study, as previously described (Uus et al., 2022, Cromb et al., 2023).

Cerebral substrate delivery categorisation

To explore the hypothesis that impaired cerebral substrate delivery plays a major role in the neurodevelopmental abnormalities associated with CHD, we divided the CHD cohort into 4 groups, according to the predicted level of substrate delivery to the developing fetal brain, based on the expected consequence of the underlying cardiac defect as described previously (Cromb et al, 2023).

(A) Group 1 = Substrate content of cerebral blood is expected to be normal (n = 232 (113 male), μ = 31.81 GW $\pm$ 1.55),

(B) Group 2 = Substrate content of cerebral blood is expected to be mildly reduced (i.e. some mixing of placental and fetal systemic venous blood) (n = 67 (35 male), μ = 32.37 GW $\pm$ 1.52),

(C) Group 3 = Substrate content of cerebral blood is expected to be moderately reduced (i.e. complete mixing of placental and fetal systemic venous blood) (n = 46 (21 male), μ = 32.72 GW $\pm$ 1.74),

(D) Group 4 = Substrate content of cerebral blood is expected to be severely reduced (i.e. complete reversal of normal placental streaming) (n = 23 (12 male), μ = 33.12 GW $\pm$ 2.02)

In the absence of direct measurements of cerebral substrate delivery, cases were classified by an expert fetal cardiologist, according to the expected effect of the underlying cardiac defect on the delivery of oxygen and nutritional content of blood to the carotid arteries, and by extension, the brain. MRI-derived fetal blood flows were used where available, as described in (Lloyd et., 2021). For cases where information about the direction of blood flow at the aortic isthmus could not be derived from MRI derived fetal blood flows, and was important for CHD categorization, it was extracted from the clinical fetal echocardiogram report, acquired as per routine clinical care. In cases where a diagnosis could potentially fit into more than one category, depending on severity or underlying hemodynamics, a combination of phase contrast (with metric optimized gating), fetal flow measurements (described in Lloyd et al., 2021, Janz et al., 2010) and/or contemporaneously acquired echocardiographic data were used to assign cases individually, following assessment of the data by a fetal cardiologist (Cromb et al., 2023).

Image registration and Jacobian determinant calculation

Non-linear deformation fields were calculated to transform the native subject T2 to the age-matched template of the dHCP fetal atlas *(*https://doi.gin.g-node.org/10.12751/g-node.ysgsy1/) using ANTs Symmetric diffeomorphic image registration (Avants et al., 2008). Warps were then concatenated between native T2, the age-matched template and a 30 GW template space, which represents the median age of the cohort (Avants et al., 2008). The log Jacobian determinant was calculated on the concatenated warp, which represents the contraction and expansion of brain regions during image registration. In the resultant log Jacobian maps, higher log-Jacobian values represent brain regions that contracted during image registration (i.e., larger global and local brain volume), while smaller values represent smaller volume (Avants and Gee, 2004). The log Jacobian volumes for all subjects were concatenated to create a single 4D file, which was used as the input for the ICA (Van Rossum and Drake, 1995, Varoquaux et al., 2010).

Independent Component Analysis (ICA) of Jacobian determinants

ICA is a data-driven, blind source separation technique that extracts salient patterns embedded in the data, it reduces the dimensionality of neuroimaging data (from many thousands of individual voxels) by separating out the multivariate signal into a maximally independent set of components (Jutten & Hérault, 1991). When applied in the spatial domain to structural imaging data (the log Jacobian determinants), ICA can detect coordinated growth between spatially separated brain regions, i.e. SCNs, which are strongly associated with other clinical or demographic variables (O'Muircheartaigh et al., 2014, Douad et al., 2014, Llera et al., 2019).

A canonical ICA algorithm (Varoquaux et al., 2010) was used, implemented in python using the nilearn package (Abraham et al., 2014). The ICA algorithm transforms the input data into components (or SCNs) that represent an 'unmixing' of the signal, such that the independent components have distributions that are non-Gaussian. The optimal number of SCNs (n = 40) for this case was chosen by surveying previous literature, and to balance robustness and interpretability (Eyre et al., 2021, Vanes et al., 2021). When the ICA dimensionality was increased above 40, visual inspection of components showed a division of cortical regions and splitting bilateral components into left/right lateralised areas.

The criteria for excluding components were (a) majority of the signal occurring in edge voxels, indicating misregistration (b) sparse, randomly distributed signal with low total area. For this dataset, all components passed the exclusion threshold and were included in subsequent analyses.

To extract weights, or 'modes', for each network in each individual subject, FSL's general linear model was applied to the component maps and the Jacobian input volumes (Winkler et al., 2014, Anderson and Robinson 2001).

Application of the General Linear Model (GLM) to identify covariates of brain structure.

For each set of SCN weights, we fit a GLM, with SCN weights as the dependent variable, to test the hypothesis that age, sex, and cerebral substrate delivery were significant predictors affecting the modes of variation across the cohort.

We fit either 1A) or 1B) depending on whether the relationship between the SCN weights and GA was linear or 2nd order polynomial (determined by the Akaike Information Criterion (AIC)).

1 A) Modes ~ GA + sex + Cerebral substrate delivery

B) Modes ~ GA + GA^2 + sex + Cerebral substrate delivery

We then used a subset of the cohort, to explore the effect of cardiovascular physiology more specifically for each CHD diagnosis. We selected diagnosis categories with > 10 subjects. These included Tetralogy of Fallot (ToF) (n = 13), Transposition of the Great Arteries (TGA) (n = 22), Right Aortic Arch (RAA) (n = 88), Hypoplastic Left Heart Syndrome (HLHS) (n = 25), Double Aortic Arch (DAA) (n = 27), Coarctation (CoA(+)) (n = 58), we also included fetuses with suspected coarctation prenatally who were not shown to have this condition in the neonatal period ("false positive" or CoA (-)) (n = 47). We included the CoA(-) group in this analysis, as it has been shown previously that this group differs significantly from a healthy control population in terms of the distribution of the fetal circulation, for reasons that remain unclear (Lloyd et al., 2021). Since the purpose of this work was to investigate the effect of cerebral substrate delivery on brain maturation, this group was included in our analysis.

2 A) Modes ~ GA + sex + CHD Diagnosis

B) Modes ~ GA + GA^2 + sex + CHD Diagnosis

We used FDR correction for multiple comparisons (between 40 models, one for each SCN) to adjust the p values for all predictors before reviewing whether they were significant in each model.

Results

Participants

429 subjects met the inclusion criteria, 67 were healthy controls (30 male) and 362 were diagnosed with CHD (182 male). All fetuses were scanned between 27- and 35-weeks gestational age (GA) (Figure 1). Histograms showing the distribution of GA at scan for each group are shown in Figure 1.

A wide spectrum of CHD was represented in this cohort, including 40 different diagnoses (Figure 1, 2), which were categorised into 4 groups based on expected cerebral substrate delivery (Cromb et al., 2023), Normal = 232, Mildly reduced = 67, Moderately reduced = 46, Severely reduced = 23. The range of CHD diagnoses within each group is shown in Figure 2.

Structural covariance networks in the developing fetal CHD brain

As shown in Figure 3, we extracted 40 SCNs, each representing independent, coordinated structural development between brain regions (Figure 4). ICA was effective at extracting meaningful neuroanatomical structures, and labels were given to each SCN according to the corresponding anatomy (Figure 4). Almost all networks were either bilateral and symmetrical or had a complementary contralateral homolog component in the opposite hemisphere (Figure 4). All tissue types in the brain were represented, including deep grey matter, white matter, cortical grey matter, and CSF. Certain SCNs were isolated to a specific tissue, and others included multiple tissue types. Charting the SCN modes against gestational age shows general

maturational trends (Supplementary info), however there is considerable variability between subjects of the same age, suggesting that there are other significant sources of variation between individuals, such as the abnormal fetal hemodynamics, for a large proportion of this cohort.

Structural covariance is associated with cerebral substrate delivery.

We fitted a GLM to each set of component weightings (also referred to as 'modes') to test whether age, sex and cerebral substrate delivery were underlying sources of variation across the cohort. 35 SCNs were significantly associated with GA, 9 with sex and 14 with expected cerebral substrate delivery after FDR correction for multiple comparisons between 40 ICs ($q < 0.05$) (Table 1). When we examined each substrate delivery group compared to controls, we found significant variation between controls and CHD where cerebral substrate delivery was expected to be normal, in 3 SCNs, including the left and right frontal temporal cortex/CSF networks, and frontoparietal cortex. These networks were also significantly different between controls and groups 2 and 3 (mildly and moderately reduced). In addition, there were differences between controls and 'mildly' and 'moderately' reduced groups in the medial frontal gyrus. The 'moderately reduced' group were uniquely different from controls in the postcentral gyrus and optic chiasm, and different from the 'expected normal' group in these networks. The 'moderately reduced' group were also different from the 'expected normal' group in the anterior cingulum, thalamus, and mesencephalon networks.

There were no SCNs that have significantly different modes of variation between controls and the 'severely reduced' cerebral substrate delivery category. This might be due to a relatively small sample of fetuses in this category ($n = 23$), limiting our statistical power to detect differences in this group. However, we did find networks distinguishing the 'severely reduced' CHD group from the 'expected normal' and 'mildly reduced' groups. These networks included

the precentral gyrus, occipital cortex/CSF, cerebellum & brainstem, and thalamus/mesencephalon. No significant differences were found between the 'moderately' and 'severely' reduced groups for any of the networks.

6 of the CHD-sensitive networks included high proportions of CSF, encompassing both extra-axial and infratentorial regions, suggested altered cortical expansion of these areas. These components also explained the highest proportion of the total variance across the cohort.

We created violin plots to show the model-fitted difference between groups, when accounting for age and sex, for components where there was a significant effect of expected cerebral substrate delivery (Figure 5). This highlighted the networks for which there was a gradient, or dose-dependent effect of cerebral substrate delivery, such as both left and right frontotemporal cortex/CSF networks and the cerebellum.

The effect of specific CHD diagnoses on structural brain maturation

Given the differences in structural covariance across the brain between CHD cerebral substrate groups, we carried out a sensitivity analysis in a subset of the cohort, to explore whether specific CHD diagnoses were predictors of variation (Table 1). In this way, we could test the hypothesis that specific cardiac defects have unique and distinct effects on structural brain maturation. We used a subset of the cohort (n = 238), only including CHD diagnosis categories with > 10 subjects (see Methods). We fit a GLM with SCN weights as the dependent variable, and tested for a combined effect of age, age^2, sex and CHD diagnosis. There were 9 different SCNs where at least one of the CHD diagnosis categories explained a significant amount of the variation between individuals. The summary of SCNs that were significant for each diagnosis category after FDR correction ($q < 0.05$) are shown in Figure 5.

We found the frontoparietal network was significantly different between controls and all CHD diagnoses except for TGA (Table 1). We also found certain SCNs, where only one CHD diagnosis group was significantly different from controls. CoA (+) explained a significant proportion of the variation in the network corresponding to the medial frontal gyrus. HLHS explained a significant proportion of the variance in the postcentral gyrus, inferior frontal & superior temporal gyrus, and occipital cortex/CSF. Fetuses with ToF were uniquely different from controls in the frontotemporal cortex, medial occipital white matter, and occipital cortex. Both ToF and TGA were significant predictors of variance in the insula network.

Discussion

In this study we applied an unsupervised, data-driven analysis technique, ICA, to capture the dynamic T2w contrast changes across the fetal brain in space and time, summarising them into an interpretable set of anatomically meaningful networks, or SCNs (Comon 1994). The networks we derived correspond to recognisable structures in the fetal brain, including regions that are developmentally critical but transiently present in the fetal period, such as anterior and posterior periventricular crossroads. We used the networks to stratify the large heterogenous cohort of different CHD cases, identifying variation across the brain according to cerebral substrate delivery and specific CHD diagnosis. Of the 40 SCNs we derived, we found a significant effect of cerebral substrate delivery or CHD diagnosis in 18 of them.

The maturation of specific networks is vulnerable to the effects of reduced cerebral substrate delivery.

Previous work has demonstrated that hemodynamic alterations in fetuses with CHD contribute to abnormalities in brain development (Limperopoulos et al., 2010, Sun et al., 2015). Volumetric

differences correlate with cerebral substrate delivery in the third trimester (Peyvandi et al., 2021, Cromb et al., 2023), which represents a critical window of accelerated fetal brain growth and increased cerebral metabolic demands. A reasonable hypothesis to explain these findings is that reduced cerebral substrate delivery, secondary to altered fetal cardiovascular physiology, is a driving factor in the emergence of structural brain differences in CHD (Rudolph, 2010). In this study, we identified networks of brain regions vulnerable to the effects of altered cerebral substrate delivery which can be broadly grouped as follows, (1) Gyral areas, pre- and post-central, medial frontal (2) Thalamus & brainstem (3) Cerebellum & infratentorial CSF, (4) Cortical/CSF regions, frontoparietal, frontotemporal and occipital cortex/CSF. The sensitivity of these particular regions is congruent with results of other studies, also noting the most significant volumetric changes in CHD in the frontal lobe and the brainstem (Ortinau et al., 2019), impaired expansion of higher cortical areas (Leonetti et al., 2019), altered patterning and delayed maturation of cortical folds (Ortinau et al., 2019, Dovjak et al., 2022, Clouchoux et al., 2013, Kelly et al., 2017), abnormal cerebellar development (Dovjak et al., 2020) and enlarged CSF spaces (Limperopoulos et al., 2010, Jorgensen et al., 2018, Schellen et al., 2015, Mlczoch E et al., 2013, Brossard-Racine et al., 2014, Ng et al, 2020). Studies across multiple different cohorts, spanning a large gestational age range, between 20 weeks GA and term, have reported increased extra-axial CSF spaces in the fetal brain with CHD (Limperopoulos et al., 2010, Jorgensen et al., 2018, Schellen et al., 2015, Mlczoch E et al., 2013, Brossard-Racine et al., 2014), which has been interpreted as a general marker of delayed brain development in this population (Brossard-Racine et al., 2014).

Cerebral substrate delivery explains some but not all of the variance in CHD

We observed differences between healthy controls and CHD fetuses where cerebral substrate delivery is expected to be normal, in frontoparietal, frontotemporal and occipital cortical/CSF networks, suggesting extrinsic factors to this analysis, such as genetic and environmental

359 factors, also mediate the differences in early brain growth. Furthermore, when we explored
360 specific CHD diagnoses in a subset of the cohort, we recapitulated this result, finding CoA (-),
361 RAA, and DAA subtypes predicted the variance in the same frontoparietal cortex/CSF networks.
362 These diagnoses are considered milder forms of CHD where cerebral substrate delivery is
363 expected to be normal (Rudolph 2010). An alternative explanation for the difference in brain
364 development is genetic variation among the milder phenotypes, which has not been accounted
365 for in this analysis. Previous work has highlighted shared underlying genetic pathways between
366 the heart and brain which may account for the phenotype of altered structural brain
367 development in CHD (Unolt et al., 2018, Richards & Garg 2010). Genetic abnormalities are also
368 highly prevalent in the CHD population (Blue et al., 2017), and protein-damaging *de novo*
369 mutations have been identified for genes highly expressed in both the developing heart and
370 brain (Homsy et al., 2015, Ji et al., 2020).

371 The residual variation in brain development between individuals in this work may also be
372 mediated by differences in placental function. The parallel development between fetal and
373 maternal organs, and the shared genetic and developmental pathways between the heart, brain,
374 and placenta, are emerging as important contributing factors to the vulnerability of this patient
375 group (Steinweg et al., 2021, Rychik et al., 2018, Jones et al., 2015, Matthiesen et al., 2016).
376 Placental imaging studies have highlighted a critical relationship between placental size and
377 overall fetal growth, in both healthy and at-risk populations, suggesting that over a third of birth
378 weight variation is due to placental weight (Salafia et al., 2008). A growing body of evidence
379 implicates abnormal placental structure and function in CHD pathology (Steinweg et al., 2021,
380 Rychik et al., 2018, Jones et al., 2015, Matthiesen et al., 2016), and future work would benefit
381 from investigating these effects on the structural brain.

382 **Specific diagnoses were better predictors of variance than others.**

When examining the differences between CHD diagnoses, HLHS and ToF were the most significant predictors of variance across different networks, in 4 and 5 SCNs respectively. We found a unique effect of HLHS diagnosis on three structural networks, including the postcentral gyrus, inferior frontal and superior temporal gyrus, and occipital cortical/CSF. In ToF fetuses, the medial occipital white matter, the insula, and the frontotemporal and occipital cortex were also significantly different from healthy controls. Previous studies have also observed a severe effect on brain development in fetuses and neonates diagnosed with either ToF (Schellen et al., 2015) or HLHS (Glauser et al., 1990, Clouchoux et al., 2013). One study reported significantly reduced cardiac output in HLHS fetuses and a dose-dependent effect on delayed brain maturation (Sun et al., 2015). Our analysis also highlighted the insula network as significantly different for fetuses with ToF or TGA compared to controls, in accordance with previous work noting delayed opercular development in term infants with complex CHD (Glauser et al., 1990, Masoller et al., 2016, Ortinau et al., 2019, Peng et al., 2016). Operculation of the insula is usually complete at term (Goldstein et al., 2017), however an open operculum and exposed insular cortex have been associated with neurodevelopmental delays in CHD and more broadly in other patient populations (Mahle et al., 2000, Licht et al., 2009, Tatum et al., 1989, Chen et al., 1996). Interestingly, TGA was not significantly different from controls for any of the networks except the insula. Although previous work has shown that whole brain volume is reduced in fetuses with TGA, and disproportionately smaller than the volume of the fetal body (Jorgensen et al., 2018, Cromb et al., 2023), our results suggest that the local effects across the brain are minimal. It is plausible that although the global brain size is smaller for this subtype, coordinated growth at the local level between brain structures is normal.

CHD-sensitive networks in frontal cortical regions

Specific networks emerged as being affected by both cerebral substrate delivery and CHD diagnosis categories. These included frontoparietal, frontotemporal and occipital cortex. In the

fetal period, these networks likely represent altered volumes of CSF, in conjunction with the areal expansion and gyrification of the cortices. Previous work using a porcine model, explored the developmental processes effected by both transient and chronic disturbances in fetal oxygen delivery (Xuegang et al., 2011, Ishibashi et al., 2012, Morton et al., 2017), resolving that this may provide a mechanistic explanation for the effect of CHD on the development of higher order cortical areas. They established that inducing chronic hypoxic exposure decreases neuronal proliferation, migration, interneuron populations and overall volume in the insula and prefrontal cortices (Morton et al., 2017). In the same study, a parallel analysis of post-mortem brain tissue from infants with complex CHD revealed less mature astrocytic processes, and a depletion of neuroblasts within the subventricular zone in frontal areas (Morton et al., 2017). The authors speculate that this cellular phenotype may propagate to the level of neuronal circuits, creating an excitatory/inhibitory imbalance in the developing cortex in CHD (Morton et al., 2017). Excitatory/inhibitory imbalance has been investigated across a wide spectrum of intellectual and behavioural disabilities, potentially explaining why children with CHD show deficits in cognitive domains associated with higher order cortices (Leonetti et al., 2019).

White matter dominated networks were largely not affected by CHD diagnosis

Many white matter networks were extracted by this analysis, reflecting the growth of key white matter structures and development of fibre connectivity over the third trimester (Kostovic & Milosevic 2006, Wilson et al., 2021), including both the anterior and posterior periventricular crossroads, and the corpus callosum/cingulum components. However, in most of these networks we did not detect significant differences between CHD and the control population. Previous studies characterising white matter development in utero in fetuses with CHD (Clouchoux et al., 2013, Ortinau et al., 2018), show smaller white matter volumes, which may just reflect the overall reduction in brain size in this group. Diffusion weighted imaging (DWI) may be more appropriate to elucidate any aberrant white matter development in CHD, as

changes can be examined at the microstructural level. To the best of our knowledge, there is one previous study using in utero DWI in CHD, which suggests a group level reduction in fractional anisotropy in the body and splenium of the corpus callosum (Khan et al., 2018). However, a larger cohort of patients over a wider gestational age range is necessary to improve understanding of group level differences, as diffusion metrics show a non-linear relationship with gestational age in fetal white matter (Wilson et al., 2021).

Conclusions

Overall, this analysis framework offers an alternative approach to studying a heterogenous patient group, capturing variation associated with age, cerebral substrate delivery and CHD diagnosis. This work contributes to building a more comprehensive understanding of brain development in CHD before birth, in utero, highlighting regions that maturing differently in this vulnerable population. The significant effect of cerebral substrate delivery and CHD diagnosis on deep grey matter, cortical regions, cerebellum and CSF supports the view that a lower oxygen environment can lead to adverse neurodevelopment. However, we also demonstrate that there is a lot of variation between individuals not attributable to fetal hemodynamic alterations, supporting the hypothesis that in utero neurodevelopment in CHD is impacted by a complex combination of factors, including genetics, maternal stress, and placental function. Our unconstrained data-driven approach identified the same vulnerable brain regions as previous work (Ortinau et al., 2019, Dovak et al., 2022, Clouchoux et al., 2013, Limperopoulos et al., 2010, Jorgensen et al., 2018, Schellen et al., 2015, Claessens et al., 2019, Mlczoch E et al., 2013, Brossard-Racine et al., 2014, Glauser et al., 1990, Masoller et al., 2016, Peng et al., 2016), which was reliant on a-priori segmentations. The reproducibility of this result supports that these findings are a meaningful reflection of biological differences between the patient and control group. The results highlight the potential for neuroimaging data in the fetal period to provide biomarkers for CHD subtypes, disentangling the unique effects of different CHD

458 diagnoses on structural neurodevelopment. Earlier identification of the structural brain networks
459 that confer neurodevelopmental risk increases the likelihood of successful targeted intervention
460 to improve outcomes later in life.

461

462 **Limitations**

463 There are some important limitations to note with this study. Firstly, the distribution of
464 gestational ages between controls and fetuses with CHD was different. Although our model
465 included GA, this may still result in some false positive or false negative significant networks.
466 We were unable to discern the delivery of specific substrates, or measure substrate delivery
467 quantitatively for every fetus. The cerebral substrate delivery groups also had uneven sample
468 sizes, with a much higher proportion of subjects in the 'expected normal' group than any other
469 group. This gave us more statistical power to detect differences between group 1 and controls
470 compared to other groups, which may have led to some false negatives, as we would expect to
471 find more differences between controls and more severe forms of CHD (Group 4 cases).
472 Similarly for CHD diagnoses, more severe subtypes (TGA, ToF and HLHS) were less common,
473 therefore our statistical tests were under powered, hampering our ability to detect differences.
474 All imaging data was acquired on the same scanner, in the same hospital catchment area in
475 central London, and despite the socioeconomic and racial diversity of London, our result may
476 not be generalizable to other populations.

477

478 **Acknowledgments**

479 We would like to thank all the families who participated in this research. We would also like to
480 thank the research radiologists, radiographers, and staff from the Evelina London Children's
481 Hospital Fetal and Paediatric Cardiology Departments and the Centre for the Developing Brain

at King's College London. Ethical approval for this study was provided by The National Research Ethics Service West London (07/H0707/105, 14/LO/1806, 17/LO/0292).

Sources of Funding

This research was funded by the Medical Research Council UK (MR/L011530/1 and MR/V002465/1) and a Wellcome Trust IEH Award (102431). This research was supported by core funding from the Wellcome/EPSRC Centre for Medical Engineering (WT203148/Z/16/Z), and by the National Institute for Health Research (NIHR) Biomedical Research Centre based at Guy's and St Thomas' NHS Foundation Trust and King's College London. The views expressed are those of the authors and not necessarily those of the NHS, the NIHR or the Department of Health.

Disclosures

The authors declare no conflict of interest.

References

A. Richards, A. and Garg, V. (2010) 'Genetics of Congenital Heart Disease', *Current Cardiology Reviews*, 6(2), pp. 91–97. Available at: https://doi.org/10.2174/157340310791162703.

Abraham, A. *et al.* (2014) 'Machine learning for neuroimaging with scikit-learn', *Frontiers in Neuroinformatics*, 8. Available at: https://doi.org/10.3389/fninf.2014.00014.

Abu-Rustum, R. *et al.* (2016) 'Are There Head Volume Alterations at 11 to 14 Weeks in Fetuses with Congenital Heart Defects? A First Trimester Case Series', *American Journal of Perinatology Reports*, 06(02), pp. e232–e238. Available at: https://doi.org/10.1055/s-0036-1584241.

503 Anderson, M.J. and Robinson, J. (2001) 'Permutation Tests for Linear Models', *Australian &*
504 *New Zealand Journal of Statistics*, 43(1), pp. 75–88. Available at: https://doi.org/10.1111/1467-
505 842X.00156.

506 Andescavage, N.N. and Limperopoulos, C. (2021) 'Placental abnormalities in congenital heart
507 disease', *Translational Pediatrics*, 10(8), pp. 2148–2156. Available at:
508 https://doi.org/10.21037/tp-20-347.

509 Avants, B. *et al.* (2008) 'Symmetric diffeomorphic image registration with cross-correlation:
510 Evaluating automated labeling of elderly and neurodegenerative brain', *Medical Image Analysis*,
511 12(1), pp. 26–41. Available at: https://doi.org/10.1016/j.media.2007.06.004.

512 Avants, B. and Gee, J.C. (2004) 'Geodesic estimation for large deformation anatomical shape
513 averaging and interpolation', *NeuroImage*, 23, pp. S139–S150. Available at:
514 https://doi.org/10.1016/j.neuroimage.2004.07.010.

515 Bassett, D.S. *et al.* (2008) 'Hierarchical Organization of Human Cortical Networks in Health and
516 Schizophrenia', *The Journal of Neuroscience*, 28(37), pp. 9239–9248. Available at:
517 https://doi.org/10.1523/JNEUROSCI.1929-08.2008.

518 Bellinger, D.C. *et al.* (2011) 'Adolescents with d-transposition of the great arteries corrected with
519 the arterial switch procedure: neuropsychological assessment and structural brain imaging',
520 *Circulation*, 124(12), pp. 1361–1369. Available at:
521 https://doi.org/10.1161/CIRCULATIONAHA.111.026963.

522 Block, A.J. *et al.* (2010) 'Clinically silent preoperative brain injuries do not worsen with surgery in
523 neonates with congenital heart disease', *The Journal of Thoracic and Cardiovascular Surgery*,
524 140(3), pp. 550–557. Available at: https://doi.org/10.1016/j.jtcvs.2010.03.035.

525 Blue, G.M. *et al.* (2017) 'Advances in the Genetics of Congenital Heart Disease', *Journal of the*
526 *American College of Cardiology*, 69(7), pp. 859–870. Available at:
527 https://doi.org/10.1016/j.jacc.2016.11.060.

528 Bonthrone, A.F. *et al.* (2021) 'Individualized brain development and cognitive outcome in infants
529 with congenital heart disease', *Brain Communications*, 3(2), p. fcab046. Available at:
530 https://doi.org/10.1093/braincomms/fcab046.

531 Bouma, B.J. and Mulder, B.J.M. (2017) 'Changing Landscape of Congenital Heart Disease',
532 *Circulation Research*, 120(6), pp. 908–922. Available at:
533 https://doi.org/10.1161/CIRCRESAHA.116.309302.

534 Brossard-Racine, M. *et al.* (2014) 'Prevalence and Spectrum of In Utero Structural Brain
535 Abnormalities in Fetuses with Complex Congenital Heart Disease', *American Journal of*
536 *Neuroradiology*, 35(8), pp. 1593–1599. Available at: https://doi.org/10.3174/ajnr.A3903.

537 Butler, S.C. *et al.* (2022) 'Neurological features in infants with congenital heart disease',
538 *Developmental Medicine & Child Neurology*, 64(6), pp. 762–770. Available at:
539 https://doi.org/10.1111/dmcn.15128.

540 Chen, C.Y. *et al.* (1996) 'MR of the cerebral operculum: abnormal opercular formation in infants
541 and children', *AJNR. American journal of neuroradiology*, 17(7), pp. 1303–1311.

542 Claessens, N.H.P. *et al.* (2018) 'Perioperative neonatal brain injury is associated with worse
543 school- age neurodevelopment in children with critical congenital heart disease', *Developmental*
544 *Medicine & Child Neurology*, 60(10), pp. 1052–1058. Available at:
545 https://doi.org/10.1111/dmcn.13747.

546 Clouchoux, C. *et al.* (2012) 'Normative fetal brain growth by quantitative in vivo magnetic
547 resonance imaging', *American Journal of Obstetrics and Gynecology*, 206(2), p. 173.e1-173.e8.
548 Available at: https://doi.org/10.1016/j.ajog.2011.10.002.

549 Clouchoux, C. *et al.* (2013) 'Delayed Cortical Development in Fetuses with Complex Congenital
550 Heart Disease', *Cerebral Cortex*, 23(12), pp. 2932–2943. Available at:
551 https://doi.org/10.1093/cercor/bhs281.

552 Comon, P. (1994) 'Independent component analysis, A new concept?', *Signal Processing*,
553 36(3), pp. 287–314. Available at: https://doi.org/10.1016/0165-1684(94)90029-9.

554 Cromb, D. *et al.* (2023) 'Total and Regional Brain Volumes in Fetuses With Congenital Heart
555 Disease', *Journal of Magnetic Resonance Imaging*, p. jmri.29078. Available at:
556 https://doi.org/10.1002/jmri.29078.

557 De Asis-Cruz, J. *et al.* (2015) 'Functional properties of resting state networks in healthy full-term
558 newborns', *Scientific Reports*, 5(1), p. 17755. Available at: https://doi.org/10.1038/srep17755.

559 Dolk, H. *et al.* (2011) 'Congenital Heart Defects in Europe: Prevalence and Perinatal Mortality,
560 2000 to 2005', *Circulation*, 123(8), pp. 841–849. Available at:
561 https://doi.org/10.1161/CIRCULATIONAHA.110.958405.

562 Douaud, G. *et al.* (2014) 'A common brain network links development, aging, and vulnerability to
563 disease', *Proceedings of the National Academy of Sciences*, 111(49), pp. 17648–17653.
564 Available at: https://doi.org/10.1073/pnas.1410378111.

565 Dovjak, G.O. *et al.* (2022) 'Brainstem and cerebellar volumes at magnetic resonance imaging
566 are smaller in fetuses with congenital heart disease', *American Journal of Obstetrics and*
567 *Gynecology*, 227(2), p. 282.e1-282.e15. Available at: https://doi.org/10.1016/j.ajog.2022.03.030.

568 Eyre, M. *et al.* (2021) 'The Developing Human Connectome Project: typical and disrupted
569 perinatal functional connectivity', *Brain*, 144(7), pp. 2199–2213. Available at:
570 https://doi.org/10.1093/brain/awab118.

571 Fenchel, D. *et al.* (2020) 'Development of Microstructural and Morphological Cortical Profiles in
572 the Neonatal Brain', *Cerebral Cortex*, 30(11), pp. 5767–5779. Available at:
573 https://doi.org/10.1093/cercor/bhaa150.

574 Geng, X. *et al.* (2016) 'Structural and Maturational Covariance in Early Childhood Brain
575 Development', *Cerebral Cortex*, p. bhw022. Available at: https://doi.org/10.1093/cercor/bhw022.

576 Gertsvolf, N. *et al.* (2018) 'Association between Subcortical Morphology and Cerebral White
577 Matter Energy Metabolism in Neonates with Congenital Heart Disease', *Scientific Reports*, 8(1),
578 p. 14057. Available at: https://doi.org/10.1038/s41598-018-32288-3.

579 Glauser, T.A. *et al.* (1990) 'Congenital Brain Anomalies Associated With the Hypoplastic Left
580 Heart Syndrome', *Pediatrics*, 85(6), pp. 984–990. Available at:
581 https://doi.org/10.1542/peds.85.6.984.

582 Goff, D.A. *et al.* (2014) 'Risk factors for preoperative periventricular leukomalacia in term
583 neonates with hypoplastic left heart syndrome are patient related', *The Journal of Thoracic and*
584 *Cardiovascular Surgery*, 147(4), pp. 1312–1318. Available at:
585 https://doi.org/10.1016/j.jtcvs.2013.06.021.

586 Goldstein, I.S. *et al.* (2017) 'The Lateral Temporal Lobe in Early Human Life', *Journal of*
587 *Neuropathology & Experimental Neurology*, 76(6), pp. 424–438. Available at:
588 https://doi.org/10.1093/jnen/nlx026.

He, Y., Chen, Z. and Evans, A. (2008) 'Structural Insights into Aberrant Topological Patterns of Large-Scale Cortical Networks in Alzheimer's Disease', *The Journal of Neuroscience*, 28(18), pp. 4756–4766. Available at: https://doi.org/10.1523/JNEUROSCI.0141-08.2008.

Heinze, K. *et al.* (2015) 'Discrete Alterations of Brain Network Structural Covariance in Individuals at Ultra-High Risk for Psychosis', *Biological Psychiatry*, 77(11), pp. 989–996. Available at: https://doi.org/10.1016/j.biopsych.2014.10.023.

Homsy, J. *et al.* (2015) 'De novo mutations in congenital heart disease with neurodevelopmental and other congenital anomalies', *Science (New York, N.Y.)*, 350(6265), pp. 1262–1266. Available at: https://doi.org/10.1126/science.aac9396.

Hornberger, L.K. and Eckersley, L.G. (2021) 'Aortic Coarctation: The Fetal Cardiologist's Achilles Heel', *Circulation: Cardiovascular Imaging*, 14(7). Available at: https://doi.org/10.1161/CIRCIMAGING.121.012877.

Inversetti, A. *et al.* (2020) 'Prenatal Growth in Fetuses with Isolated Cyanotic and Non-Cyanotic Congenital Heart Defects', *Fetal Diagnosis and Therapy*, 47(5), pp. 411–419. Available at: https://doi.org/10.1159/000493938.

Ishibashi, N. *et al.* (2012) 'White matter protection in congenital heart surgery', *Circulation*, 125(7), pp. 859–871. Available at: https://doi.org/10.1161/CIRCULATIONAHA.111.048215.

Jaimes, C. *et al.* (2020) 'In vivo characterization of emerging white matter microstructure in the fetal brain in the third trimester', *Human Brain Mapping*, 41(12), pp. 3177–3185. Available at: https://doi.org/10.1002/hbm.25006.

Jansz, M.S. *et al.* (2010) 'Metric optimized gating for fetal cardiac MRI', *Magnetic Resonance in Medicine*, 64(5), pp. 1304–1314. Available at: https://doi.org/10.1002/mrm.22542.

611 Ji, W. *et al.* (2020) 'De novo damaging variants associated with congenital heart diseases
612 contribute to the connectome', *Scientific Reports*, 10(1), p. 7046. Available at:
613 https://doi.org/10.1038/s41598-020-63928-2.

614 Jones, H.N. *et al.* (2015) 'Hypoplastic left heart syndrome is associated with structural and
615 vascular placental abnormalities and leptin dysregulation', *Placenta*, 36(10), pp. 1078–1086.
616 Available at: https://doi.org/10.1016/j.placenta.2015.08.003.

617 Jørgensen, D.E.S. *et al.* (2018) 'Longitudinal Brain and Body Growth in Fetuses With and
618 Without Transposition of the Great Arteries: Quantitative Volumetric Magnetic Resonance
619 Imaging Study', *Circulation*, 138(13), pp. 1368–1370. Available at:
620 https://doi.org/10.1161/CIRCULATIONAHA.118.034467.

621 Jutten, C. and Herault, J. (1991) 'Blind separation of sources, part I: An adaptive algorithm
622 based on neuromimetic architecture', *Signal Processing*, 24(1), pp. 1–10. Available at:
623 https://doi.org/10.1016/0165-1684(91)90079-X.

624 Kelly, C.J. *et al.* (2017) 'Impaired development of the cerebral cortex in infants with congenital
625 heart disease is correlated to reduced cerebral oxygen delivery', *Scientific Reports*, 7(1), p.
626 15088. Available at: https://doi.org/10.1038/s41598-017-14939-z.

627 Kostović, I. and Jovanov-Milosević, N. (2006) 'The development of cerebral connections during
628 the first 20-45 weeks' gestation', *Seminars in Fetal & Neonatal Medicine*, 11(6), pp. 415–422.
629 Available at: https://doi.org/10.1016/j.siny.2006.07.001.

630 Kostovic, I. and Rakic, P. (1990) 'Developmental history of the transient subplate zone in the
631 visual and somatosensory cortex of the macaque monkey and human brain', *The Journal of*
632 *Comparative Neurology*, 297(3), pp. 441–470. Available at:
633 https://doi.org/10.1002/cne.902970309.

634 Kuklisova-Murgasova, M. *et al.* (2012) 'Reconstruction of fetal brain MRI with intensity matching
635 and complete outlier removal', *Medical Image Analysis*, 16(8), pp. 1550–1564. Available at:
636 https://doi.org/10.1016/j.media.2012.07.004.

637 Latal, B. (2016) 'Neurodevelopmental Outcomes of the Child with Congenital Heart Disease',
638 *Clinics in Perinatology*, 43(1), pp. 173–185. Available at:
639 https://doi.org/10.1016/j.clp.2015.11.012.

640 Leonetti, C. *et al.* (2019) 'Cortical Dysmaturation in Congenital Heart Disease', *Trends in*
641 *Neurosciences*, 42(3), pp. 192–204. Available at: https://doi.org/10.1016/j.tins.2018.12.003.

642 Li, X. *et al.* (2013) 'Age-related changes in brain structural covariance networks', *Frontiers in*
643 *Human Neuroscience*, 7. Available at: https://doi.org/10.3389/fnhum.2013.00098.

644 Licht, D.J. *et al.* (2009) 'Brain maturation is delayed in infants with complex congenital heart
645 defects', *The Journal of Thoracic and Cardiovascular Surgery*, 137(3), pp. 529–537. Available
646 at: https://doi.org/10.1016/j.jtcvs.2008.10.025.

647 Limperopoulos, C. *et al.* (2010) 'Brain Volume and Metabolism in Fetuses With Congenital Heart
648 Disease: Evaluation With Quantitative Magnetic Resonance Imaging and Spectroscopy',
649 *Circulation*, 121(1), pp. 26–33. Available at:
650 https://doi.org/10.1161/CIRCULATIONAHA.109.865568.

651 Llera, A. *et al.* (2019) 'Inter-individual differences in human brain structure and morphology link
652 to variation in demographics and behavior', *eLife*, 8, p. e44443. Available at:
653 https://doi.org/10.7554/eLife.44443.

654 Lloyd, D.F.A. *et al.* (2021) 'Analysis of 3-Dimensional Arch Anatomy, Vascular Flow, and
655 Postnatal Outcome in Cases of Suspected Coarctation of the Aorta Using Fetal Cardiac

Magnetic Resonance Imaging', *Circulation: Cardiovascular Imaging*, 14(7). Available at: https://doi.org/10.1161/CIRCIMAGING.121.012411.

Mahle, W.T. *et al.* (2002) 'An MRI study of neurological injury before and after congenital heart surgery', *Circulation*, 106(12 Suppl 1), pp. I109-114.

Marelli, A. *et al.* (2016) 'Brain in Congenital Heart Disease Across the Lifespan: The Cumulative Burden of Injury', *Circulation*, 133(20), pp. 1951–1962. Available at: https://doi.org/10.1161/CIRCULATIONAHA.115.019881.

Masoller, N. *et al.* (2016) 'Mid- gestation brain Doppler and head biometry in fetuses with congenital heart disease predict abnormal brain development at birth', *Ultrasound in Obstetrics & Gynecology*, 47(1), pp. 65–73. Available at: https://doi.org/10.1002/uog.14919.

Matthiesen, N.B. *et al.* (2016) 'Congenital Heart Defects and Indices of Placental and Fetal Growth in a Nationwide Study of 924 422 Liveborn Infants', *Circulation*, 134(20), pp. 1546–1556. Available at: https://doi.org/10.1161/CIRCULATIONAHA.116.021793.

McQuillen, P.S. *et al.* (2007) 'Temporal and Anatomic Risk Profile of Brain Injury With Neonatal Repair of Congenital Heart Defects', *Stroke*, 38(2), pp. 736–741. Available at: https://doi.org/10.1161/01.STR.0000247941.41234.90.

Mebius, M.J. *et al.* (2019) 'Growth patterns and cerebroplacental hemodynamics in fetuses with congenital heart disease', *Ultrasound in Obstetrics & Gynecology: The Official Journal of the International Society of Ultrasound in Obstetrics and Gynecology*, 53(6), pp. 769–778. Available at: https://doi.org/10.1002/uog.19102.

Mlczoch, E. *et al.* (2013) 'Structural congenital brain disease in congenital heart disease: Results from a fetal MRI program', *European Journal of Paediatric Neurology*, 17(2), pp. 153–160. Available at: https://doi.org/10.1016/j.ejpn.2012.07.004.

679 Morton, P.D. *et al.* (2017) 'Abnormal neurogenesis and cortical growth in congenital heart
680 disease', *Science Translational Medicine*, 9(374), p. eaah7029. Available at:
681 https://doi.org/10.1126/scitranslmed.aah7029.

682 Naef, N. *et al.* (2017) 'Neurodevelopmental Profiles of Children with Congenital Heart Disease
683 at School Age', *The Journal of Pediatrics*, 188, pp. 75–81. Available at:
684 https://doi.org/10.1016/j.jpeds.2017.05.073.

685 Newburger, J.W. *et al.* (2012) 'Early developmental outcome in children with hypoplastic left
686 heart syndrome and related anomalies: the single ventricle reconstruction trial', *Circulation*,
687 125(17), pp. 2081–2091. Available at: https://doi.org/10.1161/CIRCULATIONAHA.111.064113.

688 Ng, I.H.X. *et al.* (2020) 'Investigating altered brain development in infants with congenital heart
689 disease using tensor-based morphometry', *Scientific Reports*, 10(1), p. 14909. Available at:
690 https://doi.org/10.1038/s41598-020-72009-3.

691 Ortinau, C.M. *et al.* (2018) 'Prenatal to postnatal trajectory of brain growth in complex congenital
692 heart disease', *NeuroImage: Clinical*, 20, pp. 913–922. Available at:
693 https://doi.org/10.1016/j.nicl.2018.09.029.

694 Ortinau, C.M. *et al.* (2019) 'Early-Emerging Sulcal Patterns Are Atypical in Fetuses with
695 Congenital Heart Disease', *Cerebral Cortex*, 29(8), pp. 3605–3616. Available at:
696 https://doi.org/10.1093/cercor/bhy235.

697 Paladini, D. *et al.* (2021) 'Frontal lobe growth is impaired in fetuses with congenital heart
698 disease', *Ultrasound in Obstetrics & Gynecology*, 57(5), pp. 776–782. Available at:
699 https://doi.org/10.1002/uog.22127.

Peng, Q. *et al.* (2016) 'Reduced fetal brain fissures depth in fetuses with congenital heart diseases: Reduced fissures in CHD', *Prenatal Diagnosis*, 36(11), pp. 1047–1053. Available at: https://doi.org/10.1002/pd.4931.

Peyvandi, S. *et al.* (2021) 'Fetal Cerebral Oxygenation Is Impaired in Congenital Heart Disease and Shows Variable Response to Maternal Hyperoxia', *Journal of the American Heart Association*, 10(1), p. e018777. Available at: https://doi.org/10.1161/JAHA.120.018777.

Peyvandi, S. and Rollins, C. (2023) 'Fetal Brain Development in Congenital Heart Disease', *Canadian Journal of Cardiology*, 39(2), pp. 115–122. Available at: https://doi.org/10.1016/j.cjca.2022.09.020.

Ren, J., Zhu, M. and Dong, S. (2021) 'Three-Dimensional Volumetric Magnetic Resonance Imaging Detects Early Alterations of the Brain Growth in Fetuses With Congenital Heart Disease', *Journal of Magnetic Resonance Imaging*, 54(1), pp. 263–272. Available at: https://doi.org/10.1002/jmri.27526.

Rollins, C.K. *et al.* (2021) 'Regional Brain Growth Trajectories in Fetuses with Congenital Heart Disease', *Annals of Neurology*, 89(1), pp. 143–157. Available at: https://doi.org/10.1002/ana.25940.

Rudolph, A.M. (2010) 'Congenital cardiovascular malformations and the fetal circulation', *Archives of Disease in Childhood - Fetal and Neonatal Edition*, 95(2), pp. F132–F136. Available at: https://doi.org/10.1136/adc.2007.128777.

Rychik, J. *et al.* (2018) 'Characterization of the Placenta in the Newborn with Congenital Heart Disease: Distinctions Based on Type of Cardiac Malformation', *Pediatric Cardiology*, 39(6), pp. 1165–1171. Available at: https://doi.org/10.1007/s00246-018-1876-x.

722 Salafia, C.M. *et al.* (2008) 'Placental characteristics and birthweight', *Paediatric and Perinatal*
723 *Epidemiology*, 22(3), pp. 229–239. Available at: https://doi.org/10.1111/j.1365-
724 3016.2008.00935.x.

725 Schellen, C. *et al.* (2015) 'Fetal MRI detects early alterations of brain development in Tetralogy
726 of Fallot', *American Journal of Obstetrics and Gynecology*, 213(3), p. 392.e1-392.e7. Available
727 at: https://doi.org/10.1016/j.ajog.2015.05.046.

728 Seeley, W.W. *et al.* (2009) 'Neurodegenerative Diseases Target Large-Scale Human Brain
729 Networks', *Neuron*, 62(1), pp. 42–52. Available at: https://doi.org/10.1016/j.neuron.2009.03.024.

730 Spreng, R.N. and Turner, G.R. (2013) 'Structural Covariance of the Default Network in Healthy
731 and Pathological Aging', *The Journal of Neuroscience*, 33(38), pp. 15226–15234. Available at:
732 https://doi.org/10.1523/JNEUROSCI.2261-13.2013.

733 Steinweg, J.K. *et al.* (2021) 'T2* placental MRI in pregnancies complicated with fetal congenital
734 heart disease', *Placenta*, 108, pp. 23–31. Available at:
735 https://doi.org/10.1016/j.placenta.2021.02.015.

736 Sun, L. *et al.* (2015) 'Reduced Fetal Cerebral Oxygen Consumption Is Associated With Smaller
737 Brain Size in Fetuses With Congenital Heart Disease', *Circulation*, 131(15), pp. 1313–1323.
738 Available at: https://doi.org/10.1161/CIRCULATIONAHA.114.013051.

739 Tatum, W.O. *et al.* (1989) 'The open opercular sign: Diagnosis and significance', *Annals of*
740 *Neurology*, 25(2), pp. 196–199. Available at: https://doi.org/10.1002/ana.410250216.

741 Thompson, E. *et al.* (2020) 'Non-negative data-driven mapping of structural connections with
742 application to the neonatal brain', *NeuroImage*, 222, p. 117273. Available at:
743 https://doi.org/10.1016/j.neuroimage.2020.117273.

744 Unolt, M. *et al.* (2018) 'Congenital heart diseases and cardiovascular abnormalities in 22q11.2
745 deletion syndrome: From well- established knowledge to new frontiers', *American Journal of*
746 *Medical Genetics Part A*, 176(10), pp. 2087–2098. Available at:
747 https://doi.org/10.1002/ajmg.a.38662.

748 Uus, A. *et al.* (2021) *3D UNet with GAN discriminator for robust localisation of the fetal brain*
749 *and trunk in MRI with partial coverage of the fetal body*. preprint. Bioengineering. Available at:
750 https://doi.org/10.1101/2021.06.23.449574.

751 Van Rossum, G. and Drake, F.L. (2011) *The Python Language Reference Manual*. Network
752 Theory Limited (Python Manual). Available at:
753 https://books.google.co.uk/books?id=Ut4BuQAACAAJ.

754 Vanes, L. *et al.* (2022) *Longitudinal neonatal brain development and socio-demographic*
755 *correlates of infant outcomes following preterm birth*. preprint. Psychiatry and Clinical
756 Psychology. Available at: https://doi.org/10.1101/2022.08.11.22278469.

757 Vanes, L.D. *et al.* (2021) 'Associations Between Neonatal Brain Structure, the Home
758 Environment, and Childhood Outcomes Following Very Preterm Birth', *Biological Psychiatry*
759 *Global Open Science*, 1(2), pp. 146–155. Available at:
760 https://doi.org/10.1016/j.bpsgos.2021.05.002.

761 Varoquaux, G. *et al.* (2010) 'A group model for stable multi-subject ICA on fMRI datasets',
762 *NeuroImage*, 51(1), pp. 288–299. Available at:
763 https://doi.org/10.1016/j.neuroimage.2010.02.010.

764 Wilson, S. *et al.* (2021) 'Development of human white matter pathways in utero over the second
765 and third trimester', *Proceedings of the National Academy of Sciences*, 118(20), p.
766 e2023598118. Available at: https://doi.org/10.1073/pnas.2023598118.

767 Winkler, A.M. *et al.* (2014) 'Permutation inference for the general linear model', *NeuroImage*, 92,
768 pp. 381–397. Available at: https://doi.org/10.1016/j.neuroimage.2014.01.060.

769 Wu, Y. *et al.* (2022) 'In Utero MRI Identifies Impaired Second Trimester Subplate Growth in
770 Fetuses with Congenital Heart Disease', *Cerebral Cortex*, 32(13), pp. 2858–2867. Available at:
771 https://doi.org/10.1093/cercor/bhab386.

772 Xuegang, L. *et al.* (2011) 'Porcine model of congenital heart defect with decreased pulmonary
773 blood flow', *Cell Biochemistry and Biophysics*, 61(3), pp. 725–730. Available at:
774 https://doi.org/10.1007/s12013-011-9246-9.

775 Zhang, T.-N. *et al.* (2021) 'Environmental Risk Factors and Congenital Heart Disease: An
776 Umbrella Review of 165 Systematic Reviews and Meta-Analyses With More Than 120 Million
777 Participants', *Frontiers in Cardiovascular Medicine*, 8, p. 640729. Available at:
778 https://doi.org/10.3389/fcvm.2021.640729.

779

780 **Figures**

781

782

783

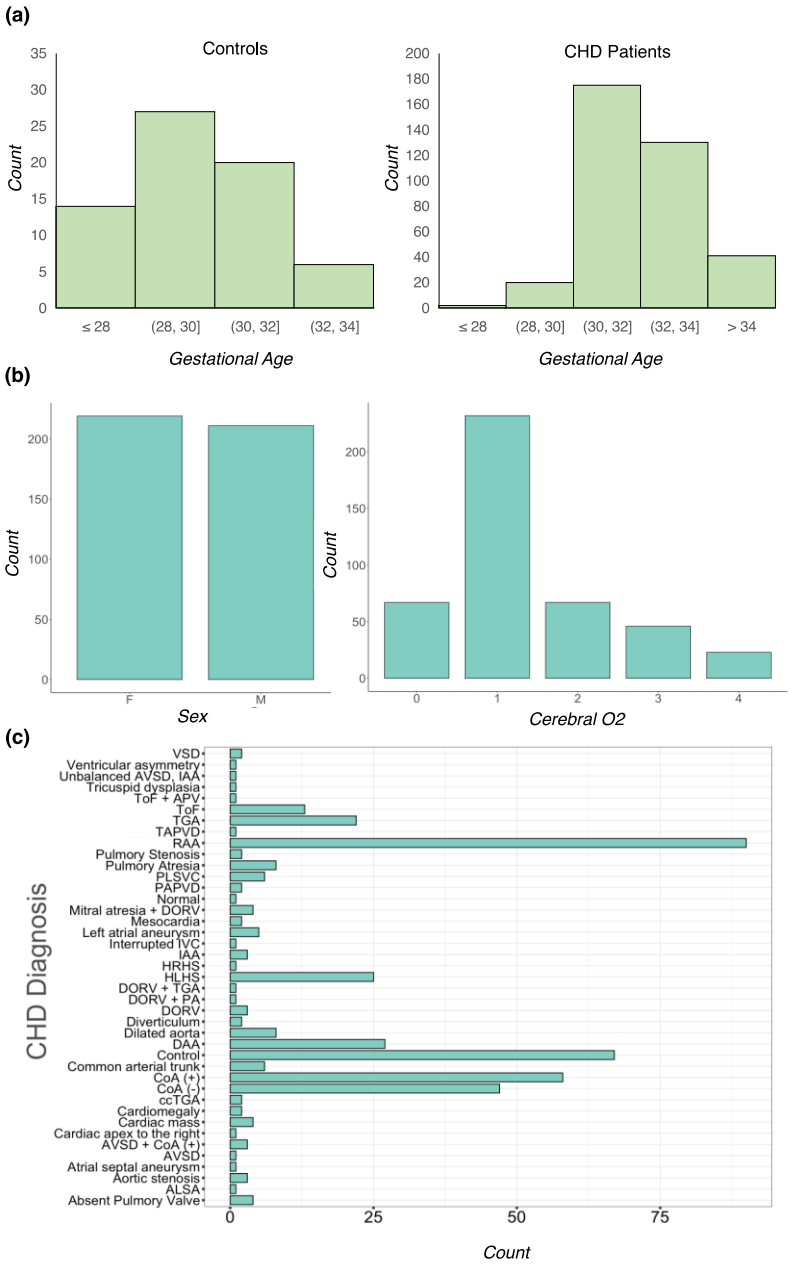

784

785 **Figure 1. Distribution of covariates and cohort information** (a) Gestational age (GA)
786 distribution for controls and CHD patient populations (b) Sex and Cerebral substrate delivery
787 grouping (0 = control, 1 = expected normal, 2 = mildly reduced, 3 = moderately reduced, 4 =
788 severely reduced). See Methods section 'CHD categorisation'. (c) Distribution of CHD
789 Diagnoses within the patient cohort.

790

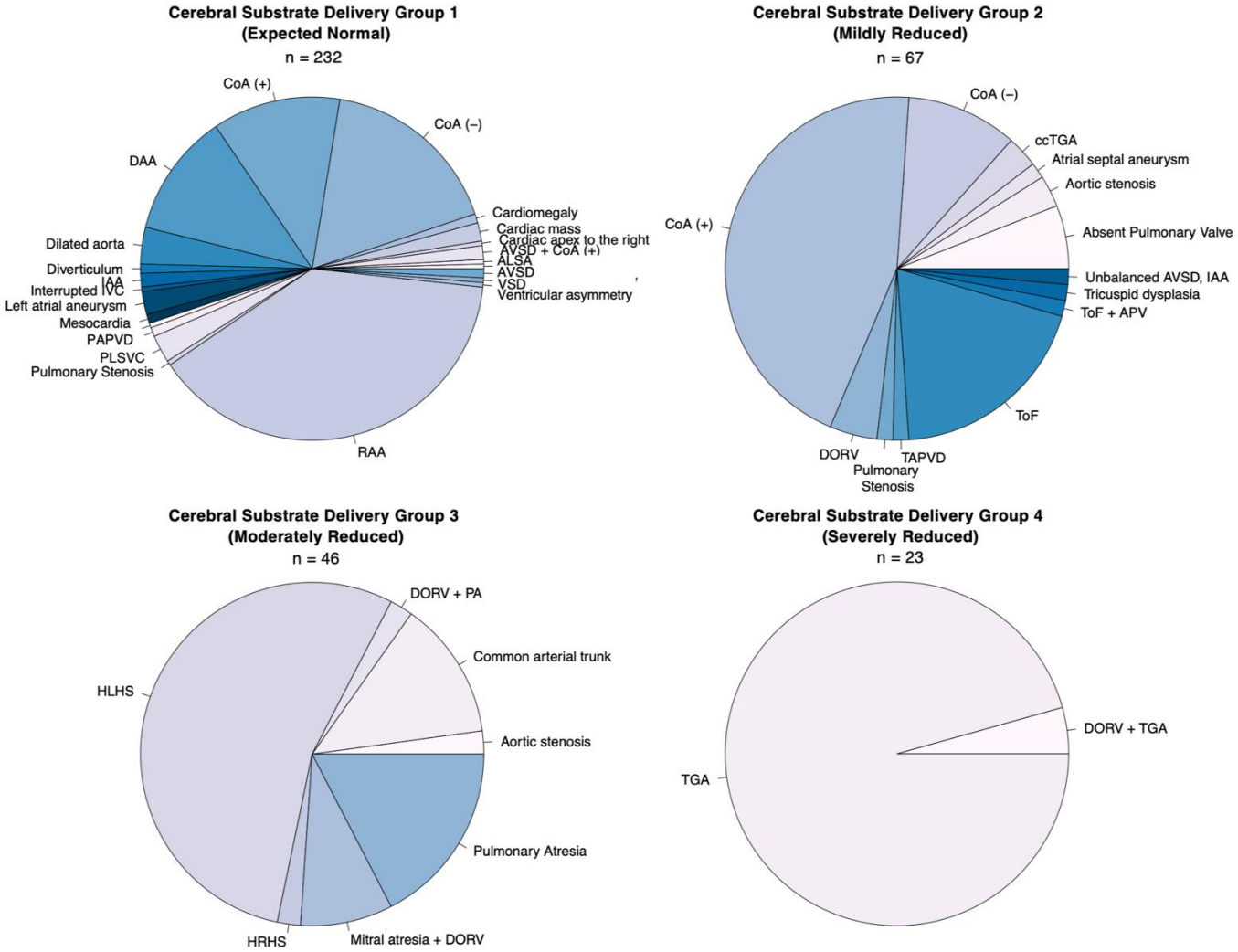

791 **Figure 2. CHD grouping according to cerebral substrate delivery** ICA separates a
792 multivariate signal (the T2w log jacobians) into additive, independent subcomponents that
793 represent brain regions covarying between individuals.

794

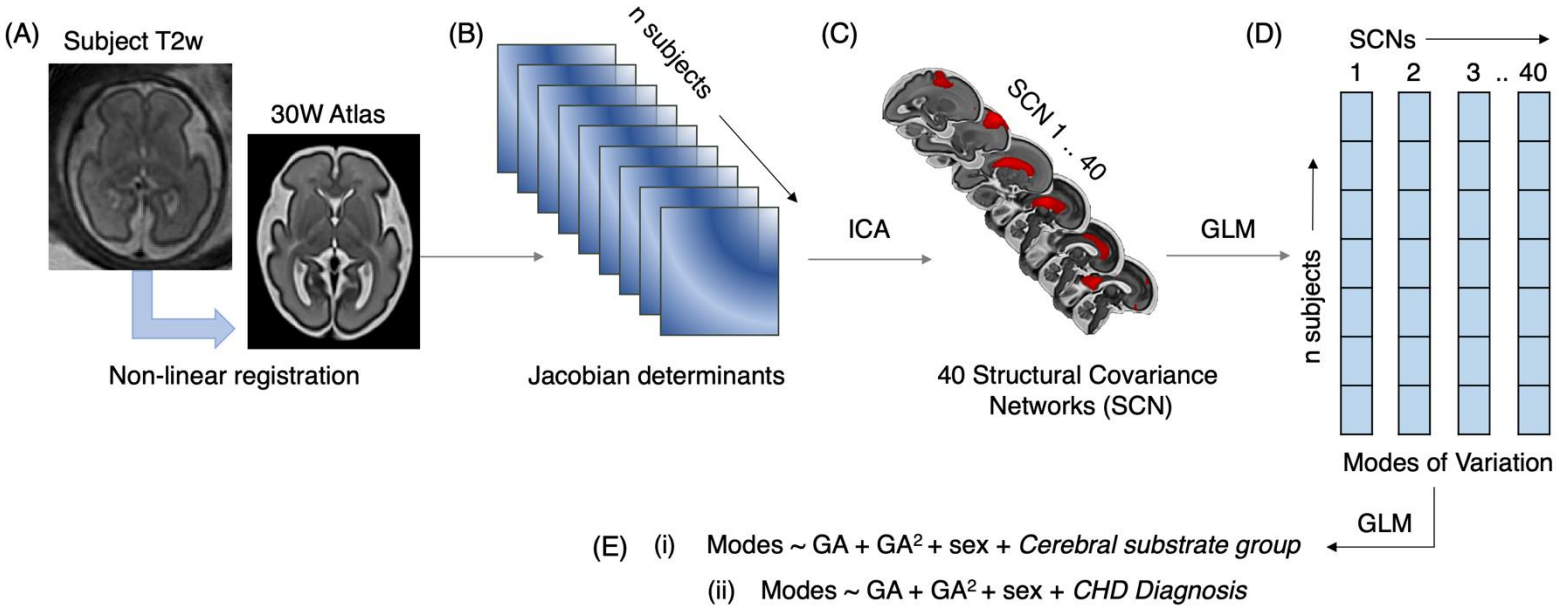

795 **Figure 3. Methods pipeline to extract Structural Covariance Networks**

796 (A) Reconstructed motion corrected T2w fetal MRI is registered to the 30 GW Atlas, using
797 non-linear registration (B) The log Jacobian of the warp is calculated (C) Jacobians are
798 concatenated across all subjects and used as input to the canonical ICA algorithm, to
799 extract 40 SCNs (D) A GLM is fit to the Jacobians & the SCNs, to extract an SCN
800 weighting (or 'modes') for each subject. (E) To examine the underlying sources of
801 variation between modes for each SCN, two GLMs were fit, testing the effect of GA,
802 GA^2, sex and either (i) cerebral substrate grouping or (ii) CHD Diagnosis.

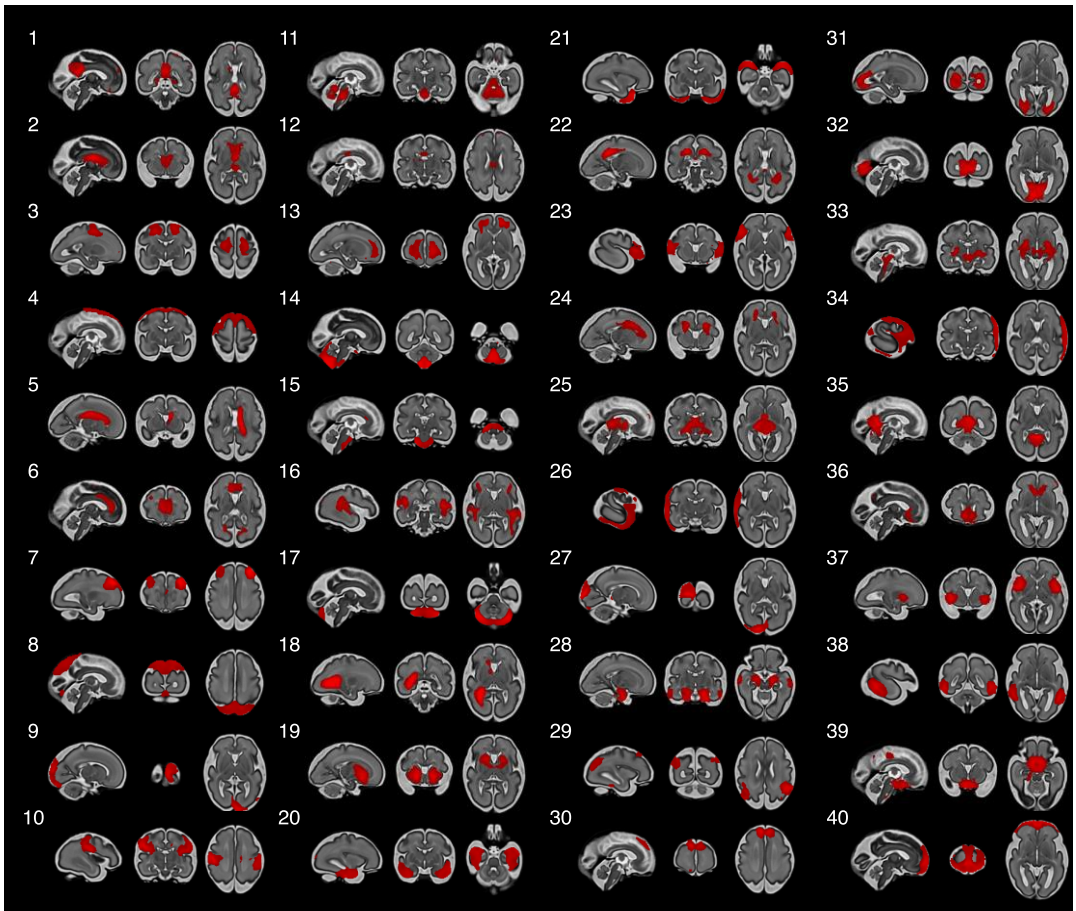

1	Splenium, posterior cingulum, precuneus, parahippocampal area
2	Frontal horn, third ventricle
3	Precentral gyrus (Motor)
4	Fronto-parietal CSF
5	Lateral ventricle (L)
6	Anterior cingulum
7	Medial frontal gyrus
8	Parieto-occipital CSF
9	Occipital CSF (L)
10	Postcentral gyrus (Sensory)
11	Cerebellum + Brainstem
12	Cingulate + corpus callosum
13	Frontal WM
14	Central posterior intratentorial CSF
15	Anterior infratentorial CSF
16	Inferior frontal gyrus, superior temporal gyrus
17	Inferior intratentorial CSF
18	Lateral ventricle (R)
19	Caudate, lentiform
20	Anterior temporal lobe

21	Anterior Temporal CSF
22	Posterior periventricular crossroads
23	Fronto-lateral CSF
24	Anterior periventricular crossroads
25	Thalamus, mesencephalon
26	Fronto-temporal CSF (R)
27	Occipital CSF (R)
28	Amygdala, medial temporal lobe
29	Posterior parietal cortex
30	Superior frontal gyrus
31	Lateral Occipital WM
32	Medial Occipital WM
33	Brainstem, mesencephalon, PLIC
34	Fronto-temporal CSF (L)
35	Superior cerebellum + lingual gyrus
36	Frontal horn
37	Insula
38	Posterior medial temporal lobe
39	Optic chiasm
40	Medial frontal CSF

803 **Figure 4. Structural covariance networks identified by ICA.** 40 independent SCNs overlayed

804 on a 30 GW fetal atlas. Table contains labels summarising their neuroanatomy.

805

						*SCN Weights ~ GA + Sex + **Cerebral Substrate Delivery Group*** (p)										*SCN Weights ~ GA + Sex + **CHD Diagnosis*** (p)						
SCN	Anatomy	% Variance Explained	GA fit	GA Sig	Sex	Control vs. 1	Control vs. 2	Control vs. 3	Control vs. 4	1 vs. 2	1 vs. 3	1 vs. 4	2 vs. 3	2 vs. 4	3 vs 4	CoA(-)	CoA(+)	DAA	HLHS	RAA	TGA	ToF
3	Precentral gyrus (Motor)	1.74	0	0	0	0.857	0.109	0.187	0.739	0.011	0.077	0.533	0.674	0.025	0.077	0.620	0.561	0.561	0.404	0.998	0.561	0.561
4	Fronto-parietal CTX/CSF	4.27	1	1	0	0.001	0.002	0.001	0.067	0.764	0.370	0.764	0.719	0.764	0.322	0.006	0.014	0.001	0.001	0.008	0.093	0.001
5	Lateral ventricle (L)	3.68	1	1	0	0.799	0.816	0.799	0.799	0.574	0.590	0.574	0.574	0.816	0.432	0.842	0.842	0.842	0.842	0.842	0.842	0.842
6	Anterior cingulum	1.61	2	1	0	0.974	0.798	0.167	0.565	0.556	0.022	0.385	0.288	0.599	0.518	0.870	0.589	0.589	0.083	0.870	0.524	0.524
7	Medial frontal gyrus	1.25	1	1	0	0.389	0.010	0.018	0.599	0.010	0.029	0.910	0.900	0.085	0.127	0.964	0.028	0.993	0.056	0.339	0.964	0.424
9	Occipital CTX/CSF (L)	1.60	1	1	0	0.762	0.010	0.762	0.766	0.002	0.897	0.691	0.014	0.008	0.762	0.745	0.320	0.818	0.818	0.818	0.818	0.012
10	Postcentral gyrus (Sensory)	1.72	1	1	0	0.244	0.122	0.019	0.244	0.326	0.036	0.513	0.262	0.879	0.265	0.519	0.377	0.492	0.037	0.519	0.377	0.816
11	Cerebellum + Brainstem	3.91	1	1	1	0.253	0.253	0.814	0.263	0.465	0.155	0.036	0.082	0.020	0.336	0.258	0.518	0.412	0.258	0.258	0.258	0.962
14	Cerebellum/ Intratentorial CTX/CSF	2.82	2	1	1	0.518	0.411	0.712	0.518	0.002	0.216	0.170	0.250	0.697	0.712	0.796	0.832	0.832	0.832	0.832	0.796	0.407
16	Inferior frontal gyrus, superior temporal gyrus	1.35	1	1	0	0.553	0.704	0.263	0.104	0.700	0.454	0.144	0.377	0.128	0.292	0.879	0.879	0.102	0.015	0.343	0.102	0.343
25	Thalamus, mesencephalon	1.71	2	1	1	0.755	0.347	0.268	0.268	0.056	0.038	0.038	0.592	0.415	0.592	0.675	0.675	0.833	0.675	0.833	0.675	0.675
26	Fronto-temporal CTX/CSF (R)	5.12	1	1	0	0.025	0.025	0.025	0.274	0.397	0.397	0.730	0.926	0.457	0.443	0.189	0.424	0.424	0.057	0.057	0.424	0.990
27	Occipital CTX/CSF (R)	1.62	1	1	0	0.127	0.237	0.122	0.311	0.925	0.560	0.925	0.563	0.973	0.438	0.089	0.074	0.530	0.016	0.119	0.530	0.929
32	Medial Occipital WM	2.46	2	1	0	0.095	0.095	0.013	0.439	0.650	0.142	0.650	0.280	0.650	0.104	0.191	0.118	0.761	0.052	0.426	0.571	0.021
34	Fronto-temporal CTX/CSF (L)	5.26	1	1	0	0.024	0.024	0.024	0.933	0.406	0.406	0.235	0.793	0.111	0.088	0.370	0.370	0.370	0.143	0.095	0.833	0.044
37	Insula	1.54	2	1	0	0.352	0.352	0.352	0.117	0.632	0.632	0.238	0.931	0.423	0.562	0.221	0.733	0.362	0.072	0.420	0.048	0.048
39	Optic chiasm	1.99	1	1	0	0.826	0.826	0.048	0.826	0.360	0.001	0.699	0.119	0.777	0.058	0.521	0.968	0.521	0.417	0.968	0.968	0.968
40	Medial frontal CTX/CSF	2.71	1	1	0	0.182	0.040	0.071	0.281	0.223	0.237	0.808	0.807	0.503	0.683	0.520	0.520	0.934	0.520	0.520	0.520	0.224

806

807 **Table 1. 18 SCNs where Cerebral Substrate Delivery and CHD Diagnosis are significant**
808 **predictors of variance.** Adjusted p values after FDR correction for multiple comparisons
809 between components ($q < 0.05$). Significant comparisons are indicated with coloured box. Table
810 also contains column of the proportion of total variance across the cohort explained by each
811 SCN, whether there was a relationship with GA, (0 = No relationship, 1 = linear, or 2 = 2nd order
812 polynomial), and if GA/sex were significant predictors of variance in the GLM.

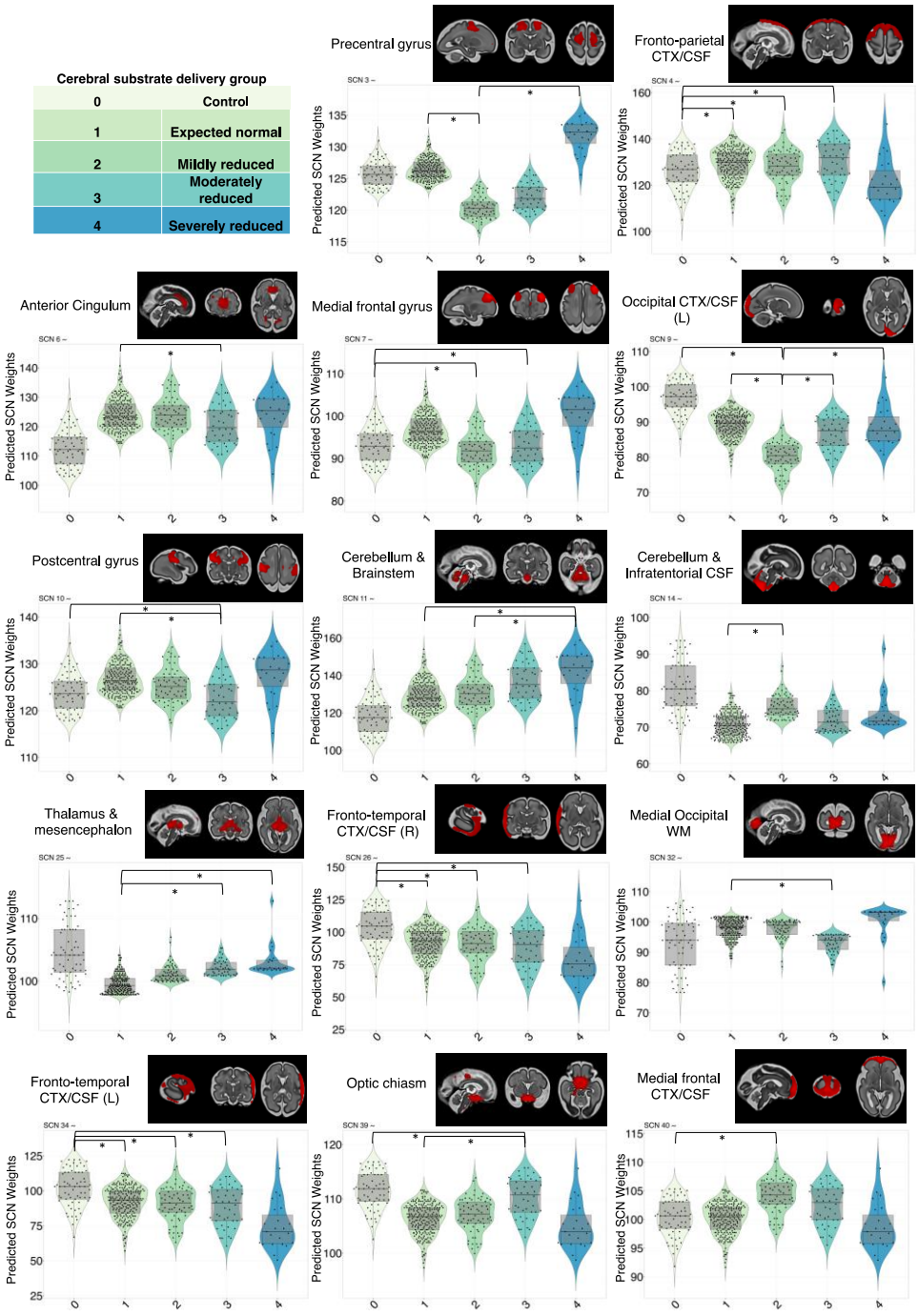

813 **Figure 5. Structural covariance explained by cerebral substrate delivery.** For each
814 significant component, the GLM predicted modes are shown (when accounting for gestational
815 age, sex and cerebral substrate delivery group), arranged along the x axis by cerebral substrate
816 delivery groups (key shown in top left hand corner). (*) denotes significant difference between
817 groups after correcting for multiple comparisons (FDR, $q < 0.05$).

818

819

820